Supplementary Information for

"Air quality improvement masks global cooling from CO_2 reductions under China's carbon neutrality policies for half a century"

Bin Zhao, Xiaochun Wang, Yuan Wang, Yisheng Sun, Da Gao, Qi Ge, Yang Gao, Junxi Zhang, Yuqiang Zhang, Drew Shindell, Steven J. Davis, Guangxing Lin, Yuhan Wang, Biwu Chu, Zhe Jiang, Hong He, Kebin He, Jiming Hao, Shuxiao Wang

Supplementary Notes

Supplementary Note 1. Relative roles of aerosol-radiation interaction (ARI) and aerosol-cloud interaction (ACI)

A rigorous assessment of the separate contributions of ARI and ACI to temperature and precipitation changes requires conducting additional fully coupled transient sensitivity simulations for multiple ensemble members, which is computationally challenging. Here we conduct additional sensitivity experiments with the atmosphere-only configuration (see Methods) to diagnose the contribution of ARI and ACI to ERF, which is closely tied to temperature changes. Supplementary Figure 9A,B reveals that ARI contributes a minor fraction of the ERF, partly because the warming effect of BC and the cooling effect of other aerosol components largely offset each other. In contrast, ACI makes a dominant contribution to ERF, implying that ACI likely plays a leading role in causing the temperature changes. Regarding precipitation, given that (1) the changes in net radiation flux at both the top of the atmosphere (TOA) and the surface due to ARI are smaller than those caused by ACI (Supplementary Figure 9), and (2) ACI can influence simulated precipitation not only through radiative effects but also by altering collision–coalescence efficiency, ACI is likely a key driver of the simulated precipitation responses.

Supplementary Note 2. In-depth discussion of spatial precipitation changes for 2050–2070

As described in the main text, the air pollutant reductions induce a strong precipitation increase in the northern tropics and a decrease in the southern tropics, along with a northward migration of the intertropical convergence zone (ITCZ)[1]. In contrast, the CO_2 reduction induces moderate precipitation decrease in the northern tropics and increase in the southern tropics, corresponding to a slight southward displacement of ITCZ.

This ITCZ shifts described in the main texts are further evidenced by changes in the meridional streamfunction (Supplementary Figure 10). The meridional streamfunction represents the structure of the Hadley circulation, with its ascending branch determining the position of the ITCZ. The ITCZ position is crucial as it defines regions of frequent precipitation, where strong atmospheric convection leads to substantial rainfall. Positive values (red) indicate clockwise circulation, while negative values (blue) represent counterclockwise circulation. Under conditions of reduced air pollutants (Supplementary Figure 10B), the ascending branch of the Hadley circulation shifts northward, corresponding to a northward displacement of the ITCZ and its associated precipitation band[2].

The changes in meridional energy transport (Supplementary Figure 11), which shows the coupling between ITCZ position and hemispheric energy redistribution, further support the above findings. Air pollutant emission reduction leads to increased southward energy transport near the equator (red line), because air pollutant reduction enhances warming in the Northern Hemisphere, creating an inter-hemispheric energy imbalance, whereby excess energy is transported from the warmer to the cooler hemisphere. In tropical regions, the Hadley circulation change facilitates this energy transport through its mechanism: air ascends in the Northern Hemisphere, flows southward at upper levels, and descends in the Southern Hemisphere. As the ITCZ position is linked to the ascending branch of the Hadley circulation, this enhanced southward energy transport corresponds to a northward ITCZ shift[3]. In contrast, CO_2 emission reduction results in an opposite but weaker northward energy transport (blue line), aligning well with a slight southward ITCZ shift.

Beyond the tropical hotspots, air pollutant reductions enhance precipitation across most of the Northern Hemisphere (14.17 mm year^{-1} on average, p-value < 0.001) while reducing precipitation in most of the Southern Hemisphere (−9.61 mm year^{-1} on average, p-value < 0.001) (Supplementary Figure 5B). Combined with a much weaker north-south contrast from CO_2 reduction (Supplementary Figure 5A), the overall CO_2 and air pollutant reductions (Supplementary Figure 5C) result in a net positive precipitation change in the Northern Hemisphere and a negative precipitation change in the Southern Hemisphere (both statistically significant with p-values < 0.001).

Beyond the global patterns, air pollutant reductions lead to a significant regional precipitation increase over China (23.33 ± 16.14 mm year^{-1}), especially over southeastern China (south of 40° N and east of 110° E, 53.75 ± 35.93 mm year^{-1}). The precipitation increase is most pronounced in spring and summer, more than tripling the changes in other seasons (Supplementary Figure 12). The precipitation increase is likely mainly driven by ACI, i.e., reduced aerosol concentrations enhance warm rain processes. In contrast, East Asian monsoon circulation does not exhibit obvious changes and is unlikely to be the primary factor behind the precipitation increase in China (Supplementary Figure 13).

Supplementary Note 3. Discussion of non-CO_2 greenhouse gases and enhanced control scenarios

The objective of this study is to assess the climate impacts of China's carbon neutrality and "Beautiful China" policies, both of which are pivotal environmental strategies for the coming decades. Since the carbon neutrality strategy specifies emission targets only for CO_2, and China has not yet established clear targets for non-CO_2 greenhouse gases such as CH_4, N_2O, and fluorinated gases, we have not considered non-CO_2 greenhouse gas control measures in this study.

It should also be noted that the carbon neutrality and "Beautiful China" strategies may have synergistic or offsetting effects on non-CO_2 greenhouse gas emissions. However, non-CO_2 greenhouse gases have relatively weak source overlaps with CO_2 and most air pollutants. The energy sector, which accounts for the vast majority of CO_2 emissions and a large portion of air pollutant emissions, contributes only about 20% of non-CO_2 greenhouse gases[4]. Agriculture contributes about 30% of non-CO_2 greenhouse gases and a large share of NH_3 emissions[4], yet the synergies and trade-offs between the two remain highly uncertain[5,6]. Other major sources of non-CO_2 greenhouse gases, including specific industrial processes (adipic acid, nitric acid, electrolytic aluminum, HFCs, etc.), waste disposal, and refrigerants, are only weakly linked to CO_2 and air pollutant emissions[4]. For these reasons, we did not consider the synergies or trade-offs of carbon neutrality and the "Beautiful China" strategies with respect to non-CO_2 greenhouse gas emissions, and we recommend that future research be conducted to further address this issue.

Beyond the carbon neutrality and clean air (CNCA) scenario described in the manuscript, we suggest that carbon neutrality should be achieved as early as possible and that negative carbon technologies be vigorously promoted in the long run, augmented by policies to rapidly reduce methane emissions. We refer to this proposed scenario as “CNCA_optimistic”. Earlier achievement of carbon neutrality and the deployment of negative emission technologies lead to a much larger cumulative carbon reduction in CNCA_optimistic relative to BAU than in CNCA relative to BAU. As a result, CNCA_optimistic realizes a net cooling effect relative to BAU earlier and with greater magnitude. In addition, the rapid methane reduction under CNCA_optimistic also contributes to cooling, further advancing and amplifying the net cooling effect. At the same time, with carbon neutrality reached earlier, air pollutant levels also decline more rapidly to minimal levels. During the period when CNCA_optimistic has achieved carbon neutrality but CNCA has not yet done so, the faster reduction of air pollutants under CNCA_optimistic may induce a slightly stronger warming effect. However, this effect will soon vanish, unlike the persistent impacts of CO_2 and methane reductions, because the atmospheric lifetimes of air pollutants and aerosols are much shorter. Therefore, compared with the BAU scenario, CNCA_optimistic is projected to produce an earlier and stronger cooling effect than CNCA. Moreover, due to earlier pollutant reductions, CNCA_optimistic can deliver greater health benefits, further highlighting the benefits of this scenario.

Supplementary Note 4. Evaluation of precipitation simulations by CESM2

Although precipitation simulation is a challenge for all global climate models, CESM2 performs much better than its predecessor in simulating historical precipitation, providing a reliable basis for long-term projections. Its global mean bias is reduced from 0.33 mm/day in CESM1 to 0.25 mm/day, with root-mean-square error decreased by about 20%[7]. These improvements mainly come from reduced wet biases in key regions like the Indian Ocean, South Pacific Convergence Zone, and tropical Atlantic ITCZ, showing better skill in large-scale water cycle processes[7].

The separate responses of precipitation to GHG and aerosol changes cannot be directly verified against observations, but these responses in CESM2 closely follow basic atmospheric energy budget constraints. Aerosol reduction causes warming, and the atmosphere balances energy by increasing latent heat release (i.e., precipitation). CO_2 reduction causes cooling, and both energy constraints and lower moisture capacity reduce precipitation. This physical rule is widely confirmed by CMIP6 models, including CESM2, showing a very strong linear relationship between global precipitation changes and surface temperature changes[8]. IPCC AR6 (Fig. 4.42) also used CESM2 as a key model to show precipitation changes under a substantial global warming[9].

In summary, CESM2's improved historical performance and physically consistent mechanisms lend confidence to the reliability of our results, despite remaining uncertainties in precipitation projections.

Supplementary Figures

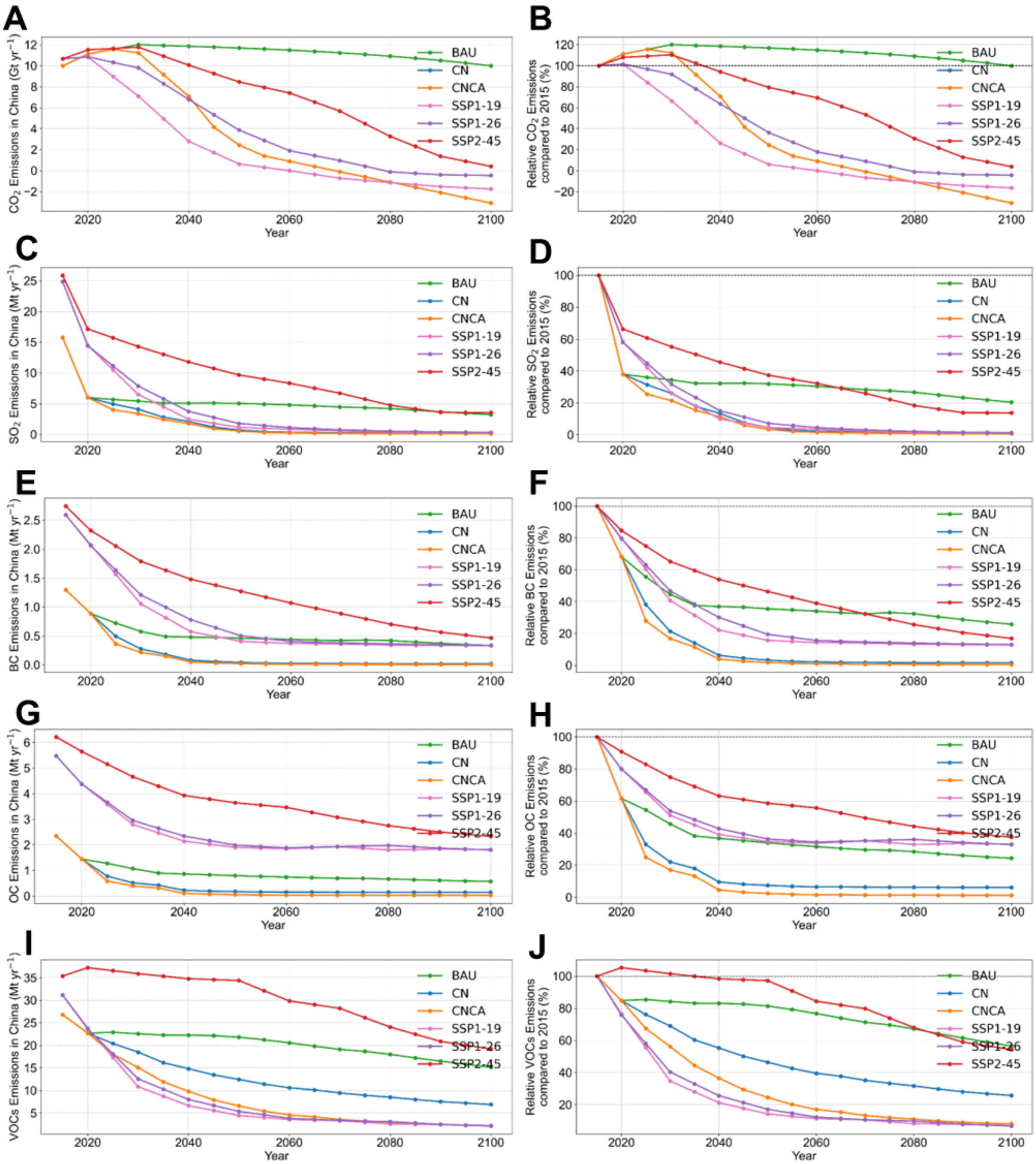

Supplementary Figure 1. National emissions of CO_2 and major air pollutants in China for 2015–2100 under the BAU and CNCA scenarios and an intermediate scenario (CN) where the carbon neutrality target is implemented but no additional clean air policies are considered. Also shown are emissions in China under different SSPs for comparison. (A, C, E, G, I) show absolute emissions, while (B, D, F, H, J) show relative changes compared with 2015. (A, B) CO_2, (C, D) SO_2, (E, F) black carbon (BC), (G, H) organic carbon (OC), and (I, J) volatile organic compounds (VOCs).

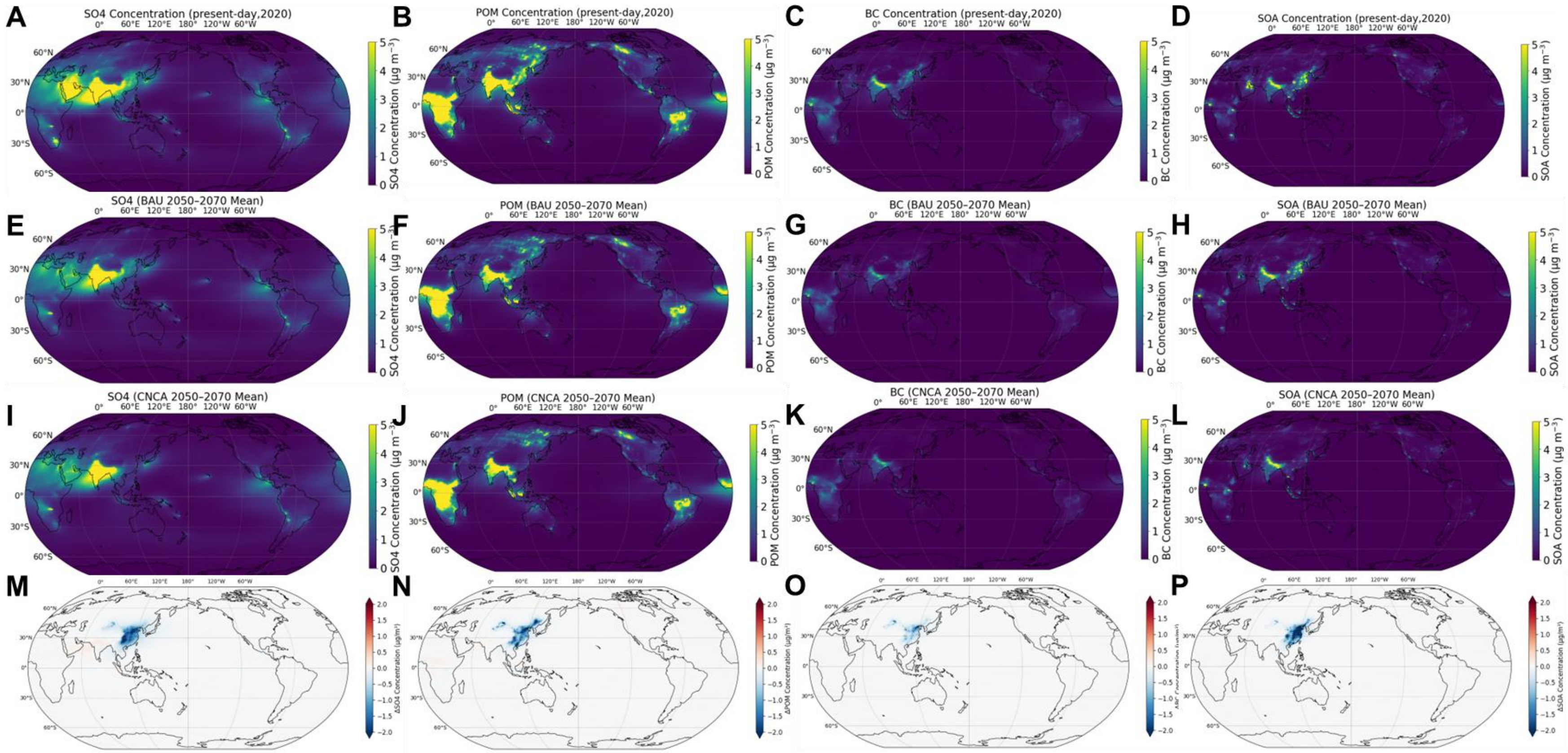

Supplementary Figure 2. Spatial distribution of concentrations and concentration differences for four $PM_{2.5}$ components (sulfate, POM, BC, and SOA) across present day (2020) and BAU/CNCA scenarios (2050–2070 mean). (A–D) Present day concentrations: (A) sulfate, (B) POM, (C) BC, and (D) SOA; (E–H) BAU scenario concentrations: (E) sulfate, (F) POM, (G) BC, and (H) SOA; (I–L) CNCA scenario concentrations: (I) sulfate, (J) POM, (K) BC, and (L) SOA; (M–P) CNCA−BAU concentration differences: (M) sulfate, (N) POM, (O) BC, and (P) SOA.

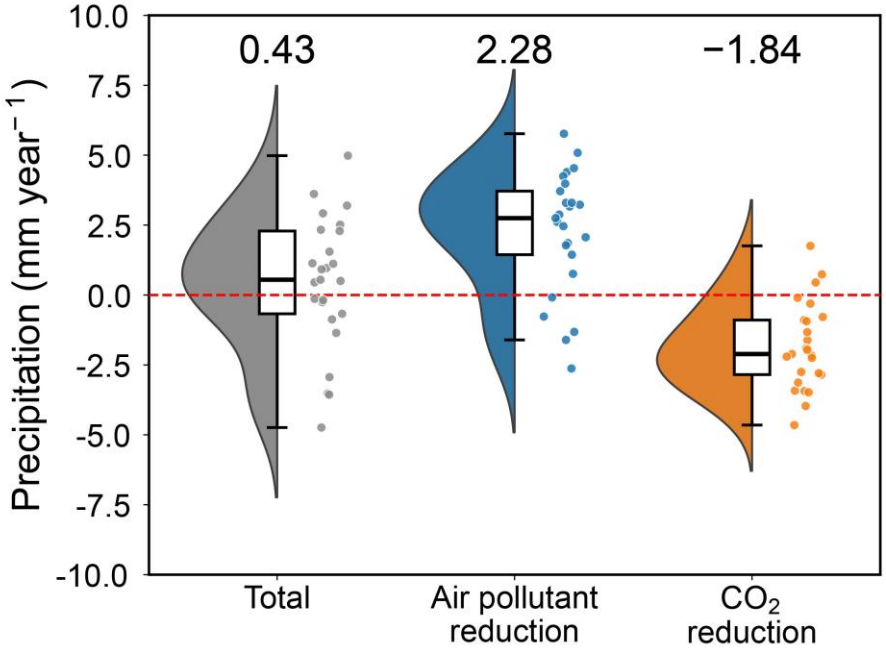

Supplementary Figure 3. Global mean differences in precipitation under China's CNCA policies with respect to the BAU scenario for 2050–2070. The panel shows the overall difference in precipitation (CNCA−BAU), as well as the respective contributions from CO_2 emission reductions (SENS−BAU) and air pollutant reductions (CNCA−SENS). Interpretation of the raincloud plots is the same as that in Fig. 1. The numbers on top of the violin plots represent mean values.

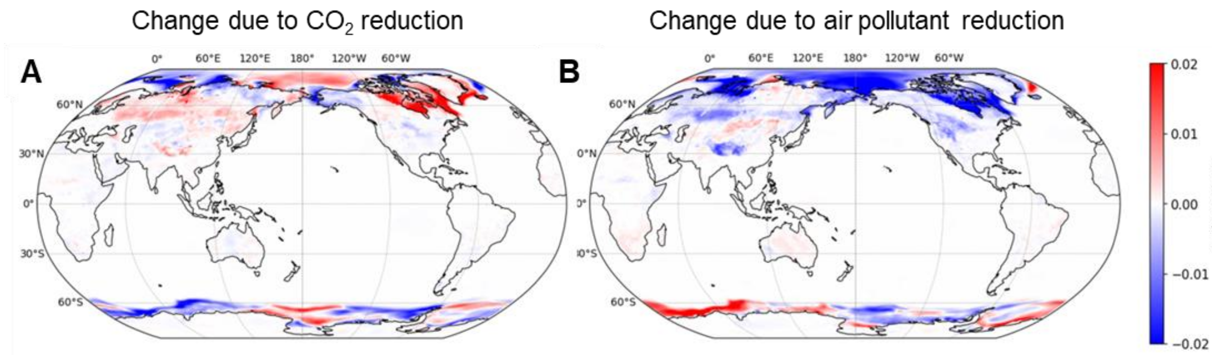

Supplementary Figure 4. Spatial distribution of the surface albedo differences under CNCA policies relative to BAU for 2050–2070. The two panels depict the differences, due to emission reductions in **(A)** CO_2 (SENS−BAU) and **(B)** air pollutants (CNCA−SENS), respectively. The albedo differences are generally opposite to temperature differences shown in Fig. 3A–B. Stippled areas indicate statistical significance at the 95% confidence level based on a two-tailed Student's t-test.

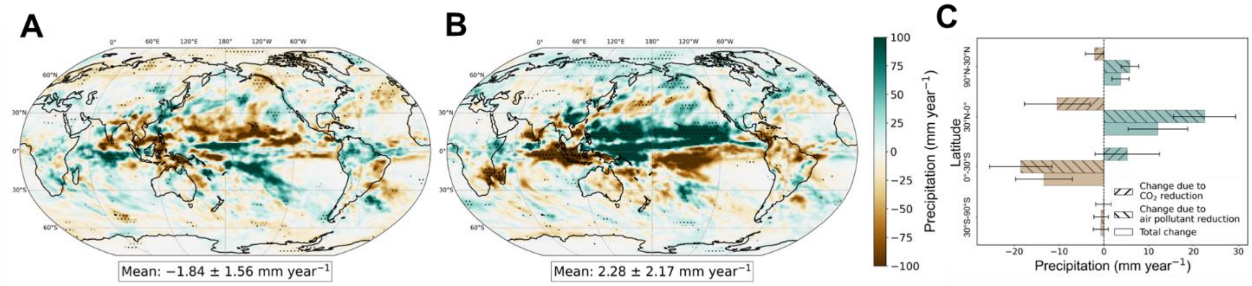

Supplementary Figure 5. Differences in precipitation under China's CNCA policies relative to the BAU scenario for 2050–2070. (A–B) Spatial distribution of precipitation differences due to emission reductions in (A) CO_2 (SENS−BAU) and (B) air pollutants (CNCA−SENS). (C) Meridional distribution of precipitation differences under the CNCA policies relative to BAU (CNCA−BAU), with contributions from CO_2 reduction (SENS−BAU) and air pollutant reductions (CNCA−SENS). Stippled areas in the spatial maps indicate statistical significance at the 95% confidence level based on a two-tailed Student's t-test. Error bars in the bar charts represent the 95% confidence intervals, also based on a two-tailed Student's t-test.

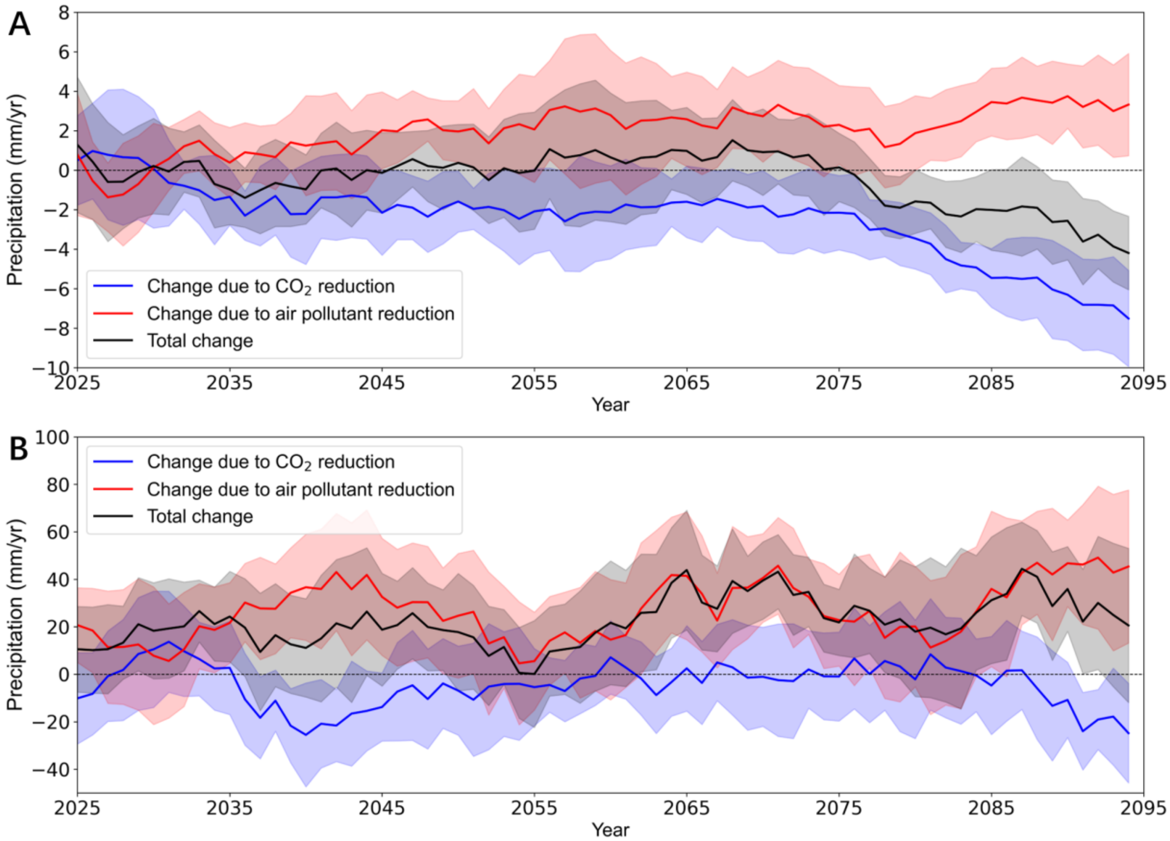

Supplementary Figure 6. Differences in precipitation caused by China's CNCA policies relative to BAU, shown as 10-year running means. (A) Global mean precipitation differences (CNCA−BAU, black), with contributions from CO_2 reduction (SENS−BAU, green) and air pollutant reductions (CNCA−SENS, red). (B) China mean precipitation differences for the same scenarios. Lines represent mean differences between scenarios, and shaded areas indicate one standard deviation of 25 samples obtained by pairwise differencing of five ensembles under the two scenarios.

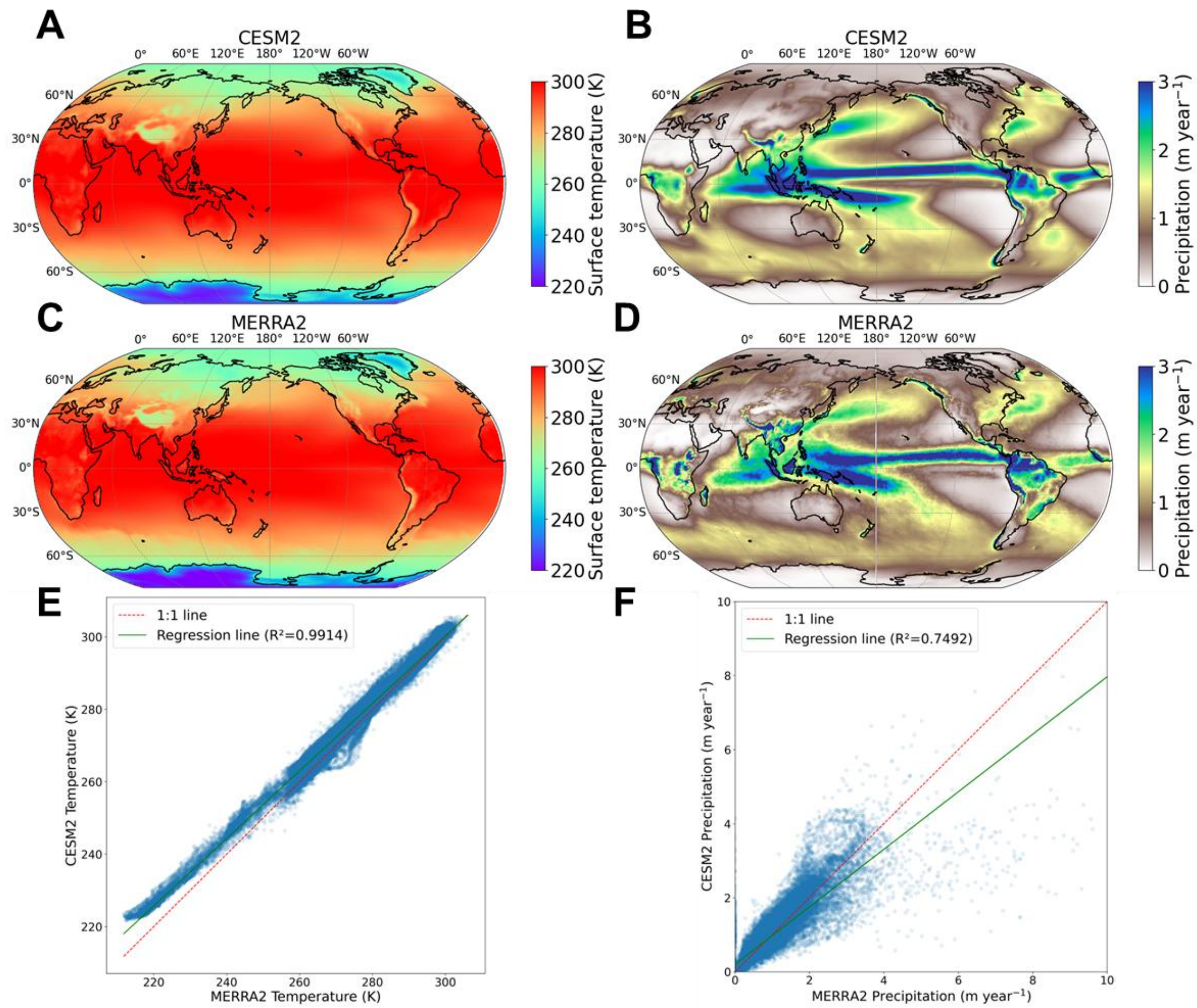

Supplementary Figure 7. Comparison of precipitation and surface temperature between CESM2 model simulation and MERRA2 reanalysis data. (A, B) Spatial distribution of surface temperature and precipitation from CESM2 model simulation for 2015–2020; **(C, D)** Spatial distribution of surface temperature and precipitation from MERRA2 reanalysis data for 2015–2020; **(E, F)** Scatter plots comparing the grid-point-based 5-year mean values between CESM2 and MERRA2 for surface temperature and precipitation, respectively. The red dashed lines represent the 1:1 line, and the green solid lines show the linear regression with corresponding R^2 values.

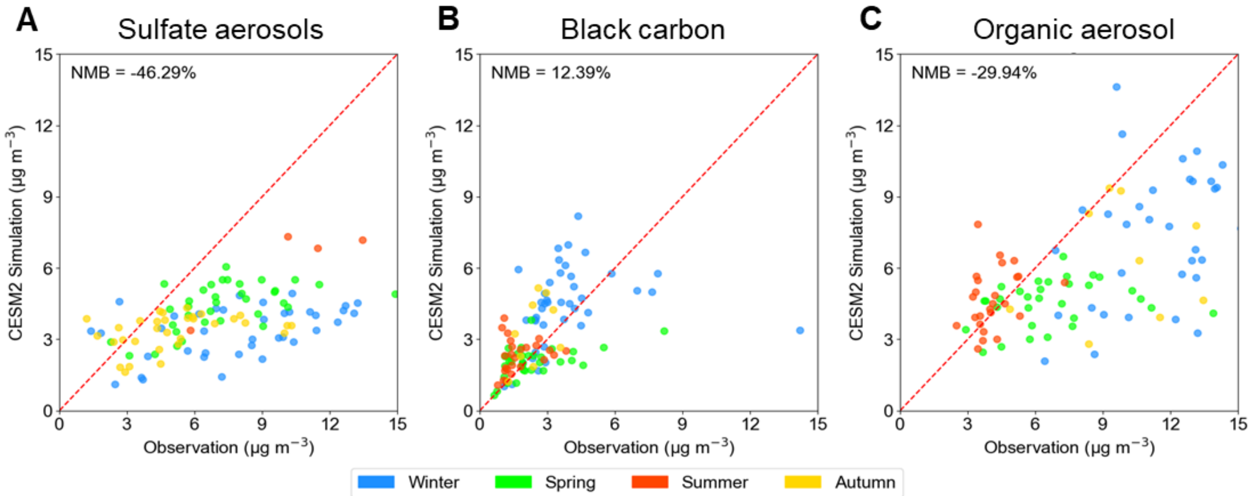

Supplementary Figure 8. Comparison of simulated concentrations of $PM_{2.5}$ chemical components with observations. (A) sulfate, **(B)** black carbon, and **(C)** organic aerosol. Observational data were collected from more than 40 component monitoring stations in the Beijing-Tianjin-Hebei region and the Dianshanhu site in Shanghai.

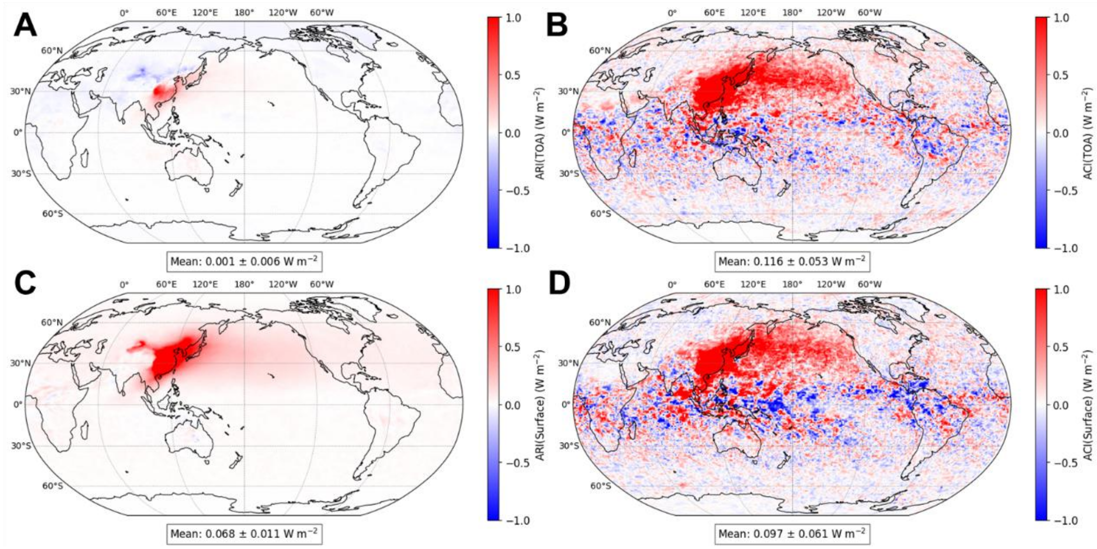

Supplementary Figure 9. Spatial contribution of aerosol-radiation interaction (ARI) and aerosol-cloud interaction (ACI) to net radiative flux changes at TOA (i.e., the ERF) and at the surface induced by air pollutant reductions under China's CNCA policies. The panels are values at (A, B) TOA and (C, D) the surface due to (A, C) ARI and (B, D) ACI, derived from atmosphere-only simulations nudged towards present-day meteorology.

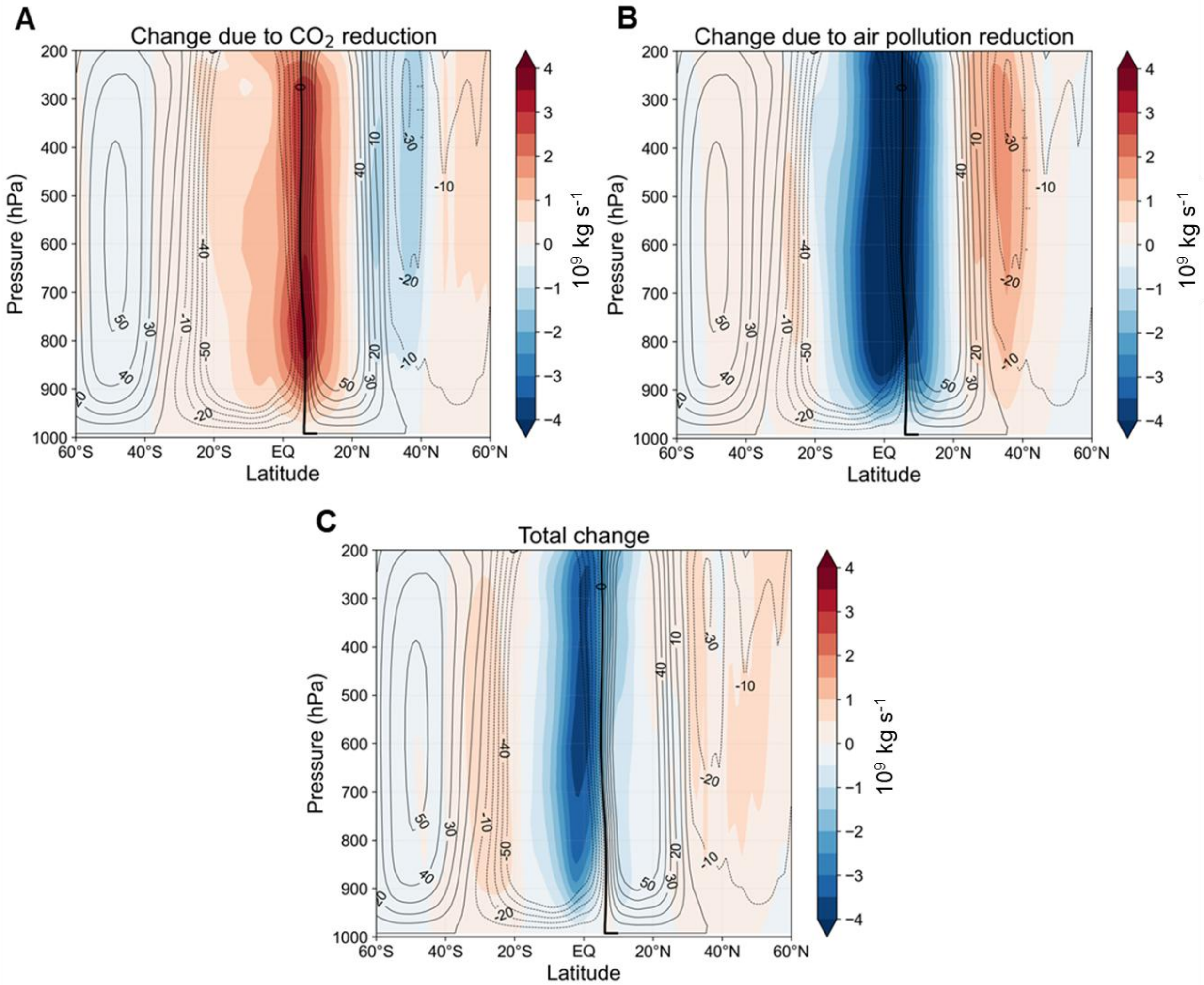

Supplementary Figure 10. Differences in meridional streamfunction showing the impacts of emission reductions on the Hadley circulation under CNCA policies relative to BAU for 2050–2070. (A) Differences due to CO_2 reduction (SENS−BAU); (B) Differences due to air pollutant reductions (CNCA−SENS); (C) Total differences (CNCA−BAU). The colored contours show differences in meridional streamfunction (10^9 kg s^{-1}). Positive (red) values indicate clockwise circulation, and negative (blue) values indicate counterclockwise circulation. The black contour lines represent the meridional streamfunction in the BAU scenario (units: 10^9 kg/s). The thick black lines indicate zero contours in the BAU state, which correspond to the ascending branch of the Hadley circulation and the climatological position of the ITCZ.

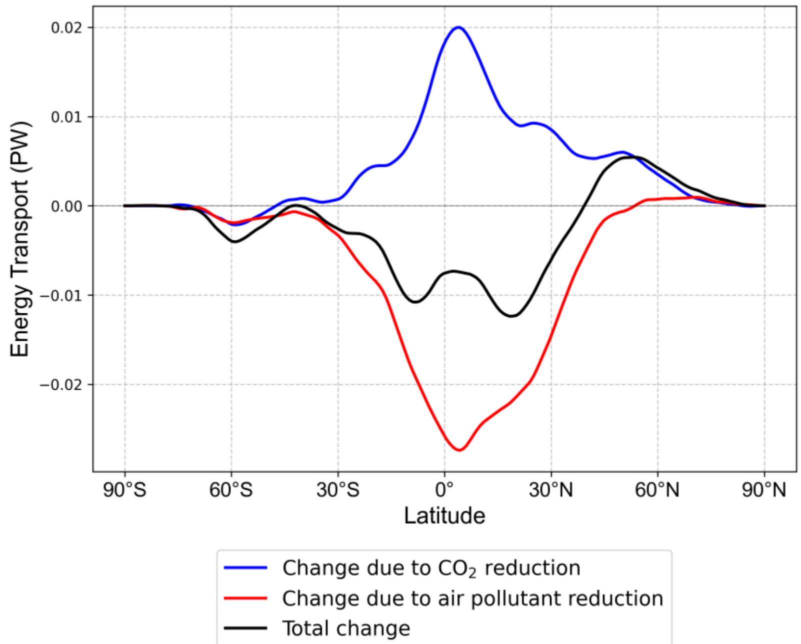

Supplementary Figure 11. Differences in the global meridional energy transport under CNCA policies relative to BAU for 2050–2070. Positive values indicate northward energy transport, while negative values indicate southward transport. The blue line shows differences due to CO_2 reduction (SENS−BAU), the red line represents differences due to air pollutant reductions (CNCA−SENS), and the black line shows the total difference (CNCA−BAU) across all latitudes from 90°S to 90°N. The energy transport is calculated based on the meridional integration of net top-of-atmosphere radiative flux (shortwave net flux minus longwave upward flux) from north to south, with appropriate latitude weighting applied.

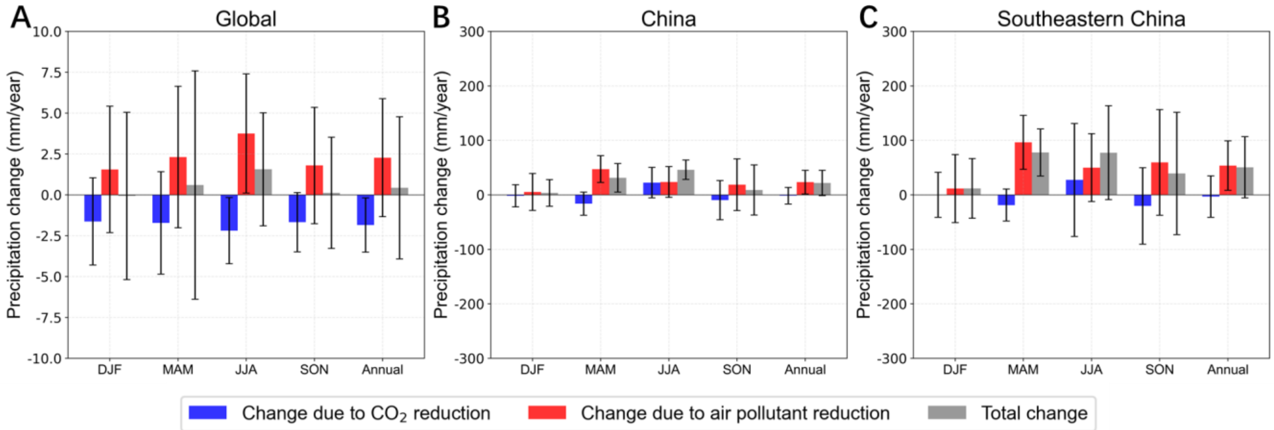

Supplementary Figure 12. Differences in annual and seasonal mean precipitation due to CNCA policies relative to BAU for 2050–2070. (A) overall differences in the world, **(B)** average differences in China, and **(C)** average differences in southeastern China (south of 40° N and east of 110° E). The four seasons are defined as DJF (December-January-February), MAM (March-April-May), JJA (June-July-August) and SON (September-October-November). The error bars indicate one standard deviation of 25 samples obtained by pairwise differencing of five ensembles under the two scenarios.

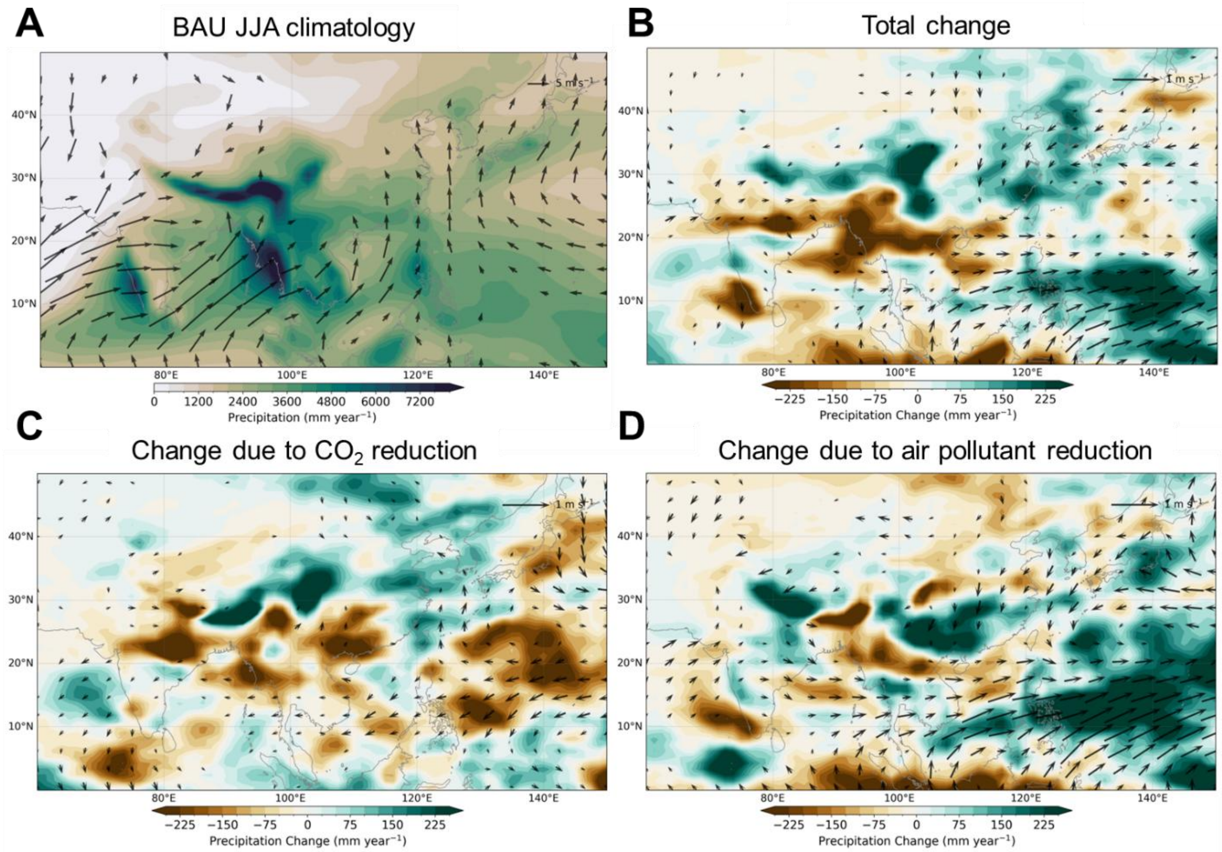

Supplementary Figure 13. Differences in JJA (June–July–August) mean precipitation and wind field in East Asia due to CNCA policies relative to BAU for 2050–2070. (A) Climatological mean precipitation and 1000hPa wind field averaged under the BAU scenario; **(B)** Total differences due to CNCA policies (CNCA−BAU); **(C)** Differences due to CO_2 reduction (SENS−BAU); **(D)** Differences due to air pollutant reductions (CNCA−SENS). Arrows indicate 1000hPa wind field, and blue (brown) shading indicates increased (decreased) precipitation in mm/year.

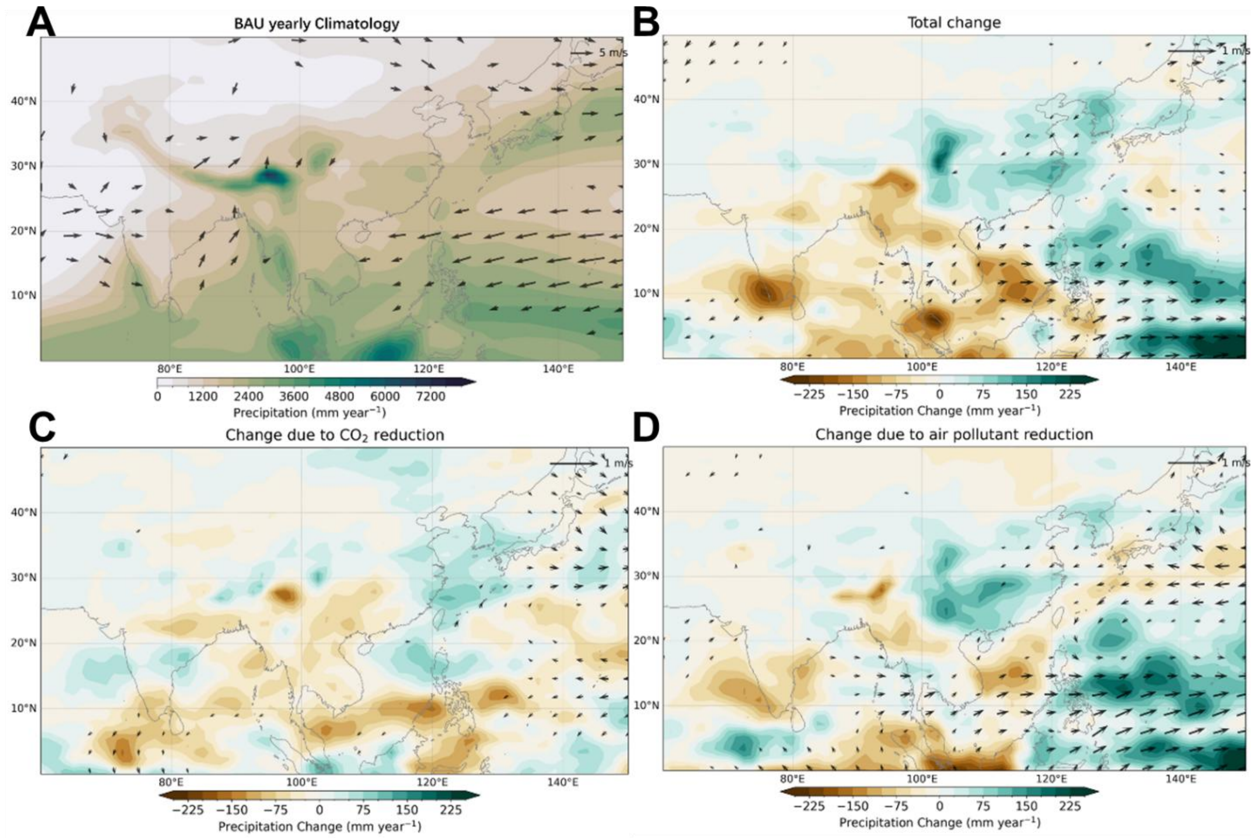

Supplementary Figure 14. The same as Supplementary Figure 13 but for annual mean precipitation.

Supplementary References

1 Navarro, J. C. A. *et al.* Future Response of Temperature and Precipitation to Reduced Aerosol Emissions as Compared with Increased Greenhouse Gas Concentrations. *J. Climate.* **30**, 939-954, doi:10.1175/jcli-d-16-0466.1 (2017).

2 Schneider, T., Bischoff, T. & Haug, G. H. Migrations and dynamics of the intertropical convergence zone. *Nature* **513**, 45-53, doi:10.1038/nature13636 (2014).

3 Donohoe, A., Marshall, J., Ferreira, D. & McGee, D. The Relationship between ITCZ Location and Cross-Equatorial Atmospheric Heat Transport: From the Seasonal Cycle to the Last Glacial Maximum. *J. Climate.* **26**, 3597-3618, doi:10.1175/jcli-d-12-00467.1 (2013).

4 He, J. K., Li, Z. & Zhang, X. L. *China's Long-Term Low-Carbon Development Strategies and Pathways*. (Springer, 2022).

5 Li, B. J. *et al.* Differentiated strategies for synergistic mitigation of ammonia and methane emissions from agricultural cropping systems in China. *Agricultural and Forest Meteorology* **358**, doi:10.1016/j.agrformet.2024.110250 (2024).

6 Hou, Y., Velthof, G. L. & Oenema, O. Mitigation of ammonia, nitrous oxide and methane emissions from manure management chains: a meta-analysis and integrated assessment. *Global Change Biology* **21**, 1293-1312, doi:10.1111/gcb.12767 (2015).

7 Danabasoglu, G. *et al.* The Community Earth System Model Version 2 (CESM2). *J. Adv. Model. Earth Syst.* **12**, e2019MS001916, doi:10.1029/2019ms001916 (2020).

8 Chai, Y. F. *et al.* Using precipitation sensitivity to temperature to adjust projected global runoff. *Environ. Res. Lett.* **16**, doi:10.1088/1748-9326/ac3795 (2021).

9 IPCC. *Climate Change 2021: The Physical Science Basis. Working Group I contribution to the Sixth Assessment Report of the Intergovernmental Panel on Climate Change*. (Cambridge University Press, 2021).